Parallel mechanism of growth of the oxide and &#945-Zr(O) layers on Zircaloy-4 oxidized in steam at high temperatures

Roland Zino, Raphaël Chosson, Maelig Ollivier, Eric Serris, Loïc Favergeon

Parallel mechanism of growth of the oxide and α-Zr(O) layers on Zircaloy-4 oxidized in steam at high temperatures

Roland ZINO [1,2], Raphaël CHOSSON [2], Maelig OLLIVIER [1], Eric SERRIS [1], Loïc FAVERGEON [1]

[1] Mines Saint-Etienne, Univ Lyon, CNRS, UMR 5307 LGF, Centre SPIN, F - 42023 Saint-Etienne France

[2] Framatome, 69456 Lyon France

Key words

Zircaloy-4, thermogravimetric analysis, kinetic modeling, steam, HT corrosion

1. Introduction

Oxidation of nuclear fuel cladding at high temperatures in steam atmosphere may occur during Loss-Of-Coolant Accidents (LOCA). This hypothetical scenario must be taken into account in safety demonstrations of Pressurized Water Reactors (PWR) in order to ensure the fuel rod integrity is maintained during the induced temperature transient and guarantee core coolability (during and after the accident scenario) [1]. In such scenario, a breach in a primary circuit coolant pipe could lead to a rapid depressurization in the reactor vessel, evaporating the water used as the primary coolant and generating a steam atmosphere. As a result, the cladding tubes heat up to temperatures over 1000 °C causing a phase transformation in the metal from α-Zr to β-Zr, an acceleration of the oxidation kinetics and oxide growth, and oxygen dissolution in the metal, stabilizing an oxygen enriched layer of α-Zr(O) [2]. The high temperature oxidation in steam atmosphere could last about 2000 s until the activation of the emergency core cooling systems (ECCS).

The kinetics of steam oxidation of zirconium alloys at high temperature has been studied extensively since the 1960s [3] and two distinct stages were generally observed. During the first one, called the pre-transition regime, the kinetic behavior is governed by a parabolic or sub-parabolic rate law describing an anionic diffusion mechanism in a dense and protective oxide layer [3–12]. The second kinetic stage generally appears after few thousand seconds of isothermal oxidation, where breakaway oxidation could occur with an increase in the oxidation rate from sub-parabolic to quasi-linear [5, 13]. The consequences of breakaway oxidation, generally appearing for temperatures between 950 and 1050 °C, are possible hydrogen absorption and oxide spallation [14, 15]. The mechanisms causing the breakaway oxidation are still unclear. Several explanations have been suggested in the literature such as the destabilizing effect of the tetragonal-to-monoclinic phase transformation in the oxide layer [11, 16, 17]. A recent study using HT XRD analysis demonstrated that this phase transformation is not the main cause of the breakaway oxidation [18]. Other hypotheses suggest that the stress relaxation in the oxide after a certain incubation time [19, 20] and the formation of an interconnected network of micro-pores can cause a direct access of the oxidizing gas to the metal/oxide interface [21, 22].

When studying the oxidation kinetics of zirconium alloys at high temperatures, the influence of steam partial pressure must be taken into account. It was reported in the literature that, for relatively low steam partial pressures, in a mixture of steam-argon for example, the phenomenon of steam starvation could occur [4, 9]. These conditions lead to the growth of a porous and non-protective oxide layer. Hydrogen blanketing could also occur if the fraction of steam in a steam-hydrogen mixture decreases below 50 %, reducing thus the overall weight gain and inducing a large hydrogen absorption [7]. According to [7, 9], when an adequate supply of steam is provided, the steam and hydrogen partial pressures have no effect on the weight gain. Moreover, when studying the oxidation of Zircaloy-4 samples in steam/argon mixtures with total pressures of 7.5 and 10 MPa, it was found that the oxidation rate is sensitive to the steam partial pressure and not to the total gas pressure [16, 23].

According to the authors, at temperatures between 900 °C and 1100 °C, the increase in steam pressure enhances the oxidation rate by altering the stability of the tetragonal phase.

Detailed physical mechanisms were proposed in the literature [24, 25] to describe the oxidation of Zircaloy-4 in steam at temperatures between 415°C and 530 °C. For example, the mechanism proposed by Tupin *et al.* [24] is based on the succession of five intermediate reactions taking place between the oxide/gas and metal/oxide interfaces with a rate determining step of diffusion. In this mechanism, the growth of the α-Zr(O) phase is not considered simply because at these temperatures, the quantity of dissolved oxygen in the metal is negligible. Lasserre [26] and Gestin [27] studied the oxidation kinetics of Zircaloy-4 at 850 °C in air and in air/steam mixtures. However, in presence of nitrogen the oxidation mechanism is altered and leads to a more severe kinetic transition due to the oxidation of zirconium nitride precipitates.

However, the existing mechanisms do not offer detailed elementary steps, describing the oxide and α-Zr(O) growth on Zircaloy-4 samples when oxidized in steam at high temperatures to the best of our knowledge.

In this study, we investigated the oxidation kinetics of Zircaloy-4 samples in steam at temperatures between 950 and 1050 °C using thermogravimetry and microstructural characterizations in order to propose a mechanism and a kinetic model revealing the dominant parameters governing the oxide and α-Zr(O) growth rates.

2. Materials and methods

2.1. Samples

The experimental samples were cut from as-received Zircaloy-4 cladding tubes provided by Framatome. The standard chemical composition of the samples is shown in Table 1. Outer diameter and thickness are equal to 10.92 mm 0.98 mm respectively. Two sets of samples of 10 mm long and 5 mm long were used. Before the oxidation tests, the surfaces of the samples were cleaned for 5 min in acetone and for 5 min in ethanol using an ultrasonic cleaner and then air-dried.

Alloying element	**Sn**	**Fe**	**Cr**	**O**	**Zr**
wt %	1.3	0.2	0.1	0.13	Bal.

Table 1 Chemical composition of Zircaloy-4 samples, in wt%.

2.2. Thermogravimetry

The oxidation behavior of Zircaloy-4 tube samples was examined by continuous recording of the weight gain – with 1-µg accuracy – during double sided oxidation, using a symmetrical thermobalance TAG-16 from SETARAM. The samples were hung in the temperature controlled isothermal zone with a sample holder made of alumina and platinum. All the experiments were preceded by furnace purging under primary vacuum for 30 min. The samples were heated at 20 °C/min under helium, maintained at the isothermal oxidation temperature for the target time and cooled in helium at about 60 °C/min down to 400 °C and then by natural cooling in helium atmosphere to room temperature. Once the target temperature was reached, a mixture of steam and helium was introduced. A steam generator Wetsys from SETARAM delivered the mixture of steam and helium with different steam partial pressures ranging from 100 to 140 hPa for a total pressure of 10^3 hPa (atmospheric pressure). The highest steam partial pressure investigated in this study was defined by the maximum capacity of the thermobalance. A total flow rate of 6 L/h (equivalent to 1.9 L/h/cm^2 when normalized to the cross-sectional area of the furnace) passing over the sample was used to avoid steam starvation [7, 9]. In order to prevent any

undesired condensation, the parts of the thermobalance in contact with steam were heated to 90 °C. Hydrogen partial pressure was the result of the hydrogen production during the isothermal oxidation and was considered negligible.

2.3. Optical microscopy

The oxidized samples were cold mounted in resin and then mechanically ground and polished to a 1200 grit finish in order to examine them using optical microscopy. The OLYMPUS Stream image analysis software allowed measurements of the oxide and α-Zr(O) thicknesses at both the outer and inner surfaces of the oxidized samples. The values reported in this study correspond to the average of 100 readings taken in four different areas covering thus the entire circumference of each sample.

2.4. Kinetic framework of the study

The goal of this study is to propose a kinetic model based on the method proposed in [28, 29] expressing the reaction rate as follows:

$$\frac{d(m/S)}{dt} = B_0 \cdot \Phi(T, P_i) \cdot S_m(t) \quad (1)$$

Where $\frac{dm/S}{dt}$ is the weight gain rate (in g/m^2/s), $\Phi(T, P_i)$ is the areic reactivity of growth (in mol/m^2/s) and $S_m(t)$ is a time dependent function (in m^2/mol) that can be expressed as a function of the dimensions of the area where the rate-determining step occurs and B_0 is a constant relative to the measured rate (in g/m^2).

This requires the validation of two major hypotheses beforehand. The first one is the steady-state approximation stating that intermediate species, such as adsorbed gas and point defects, do not accumulate during the reaction [30]. In other terms, the weight gain obtained by thermogravimetry corresponds only to the growth of the oxide and α-Zr(O) layers. The quantity of oxygen dissolved in the β-Zr phase is considered negligible relatively to that contributing to the growth of the oxide and α-Zr(O) layers. In this study, the hypothesis of a steady-state regime[1] during both pre- and post-transition stages was verified using the coupling of thermogravimetry and calorimetry which showed that the kinetic rates measured by the two methods were proportional [30].

The second essential hypothesis is the existence of a rate-determining step controlling the reaction rate. A Kinetic model considers that the global reaction is the result of a succession of elementary steps occurring at the interfaces (external and internal reactions) and in the bulk of the sample (diffusion). Each step has a different rate expression. If the rate determining assumption is verified, the global reaction rate can be expressed by Eq. (1).

This means that when a rate determining step exists, i.e. if one of the elementary steps governs the rate of the reaction, one can separate the thermodynamic variables from the time variable as shown in Eq. (1). The validation of this hypothesis can be done by conducting several jumps in temperature at different times and by verifying if the ratio of the reaction rates just before and just after each jump remains equal to a constant value [30, 31]. Since the duration of the jump is relatively small, the evolution of the $S_m(t)$ function during the jump is assumed to be negligible. As a result, the ratio of the reaction rates is equal to the ratio of the areic reactivity of growth.

The examination of temperature and partial pressures influence on the reaction kinetics was also made possible using the method of jumps. This method consists in changing rapidly at a specified time one thermodynamic parameter, e.g. temperature or gas partial pressure, allowing thus a quantitative evaluation of the kinetic response of the sample corresponding to the rate determining step [29]. A

[1] The validation of the steady state assumption is presented in the supplementary material.

heating rate of 30 °C/min was used to carry out the temperature jumps for a duration less than 300 s. As for the partial pressure jumps, two identical steam generators connected to the thermobalance via a valve system allowed a rapid switching to the target partial pressure when the desired time was reached.

2.5. Influence of the thermodynamic parameters

The influence of the thermodynamic parameters on the oxidation reaction of Zircaloy-4 in steam, i.e. temperature and partial pressures of steam and hydrogen were experimentally assessed using the method of jumps. If the reaction rate can be expressed according to Eq. (1), this means carrying out temperature jumps for example, while keeping constant steam partial pressure, allows the evaluation of the areic reactivity of growth ($\Phi(T,P)$) variation of the rate-determining step with temperature [31]. The same method was applied to quantify the influence of steam and hydrogen partial pressures.

3. Results

3.1. Global reaction rate

The oxidation of Zircaloy-4 in thermobalance in a mixture of steam and helium with 100 hPa of steam partial pressure was examined at six temperatures ranging from 950 to 1050 °C. At each temperature, 2 or 3 experiments were performed in order to assess the experimental scattering. At 1000 °C, the experiment was repeated 20 times.

Figure 1 displays the weight gain in (mg/cm^2) and the weight gain rate (mg/cm^2/min) recorded continuously at each temperature. The time axis represents the isothermal oxidation time, i.e. t = 0 s marks the introduction of the steam/helium mixture in the thermobalance and the start of the reaction. A brief acceleration of the oxidation rate as seen in Figure 1 (b) and (c) can be detected at the very beginning of the experiments. When the oxidizing mixture flows over the bare metal, it causes the sudden oxidation of the sample via the nucleation of newly formed oxide at the surface of the metal and as a result, an increase in the reaction rate can be observed on the kinetic curves. The oxidation rate begins afterwards to decrease progressively with time when a homogeneous protective oxide layer covering the whole sample is formed.

As expected, the kinetic curves at 950, 985, 1000, 1015 and 1030 °C can be broken down into two stages: a pre-transition stage characterized by the decrease of the reaction rate and a post-transition stage. The end of the pre-transition regime, i.e. the occurrence of breakaway oxidation can be easily identified as the first local minimum of the weight gain rate curves in Figure 1 (b) and (c). Figure 1 (d) displays the weight gain variation with time in a log-log scale. Assuming that the weight gain can be expressed by the empirical power law as $\left(\frac{\Delta m}{S}\right)^n = k \times t$, with k (in (mg/cm^2)^n/s) being the kinetic parameter, the exponent n deduced from Figure 1 (d) can reveal the general tendency of the kinetic curves. The average exponents n at different temperatures are presented in Table 2. In the pre-transition stage, the kinetic curves seem to follow a parabolic law except at 950 °C, where a quasi-cubic law is followed.

The transition times to breakaway and the corresponding transition weight gains in Table 2 were measured and are in accordance with the literature [10, 13, 32–35]. In order to obtain some statistical data and more precision on the transition time to breakaway oxidation at 1000 °C, the experiment was repeated 20 times. The post-transition kinetic curves seem to follow a quasi-linear law or a succession of quasi-parabolic laws.

At 1050 °C, breakaway oxidation did not occur and the reaction rate seems to follow a sub-parabolic law during the whole oxidation time.

The results show the non-monotonic dependence of the transition time to breakaway with temperature as previously reported by Leistikow *et al.* [4]. This could be caused by a combination of phenomena occurring simultaneously in this temperature range like creep in the different layers, phase transformation in the oxide, stress relaxation and segregation of the alloying elements.

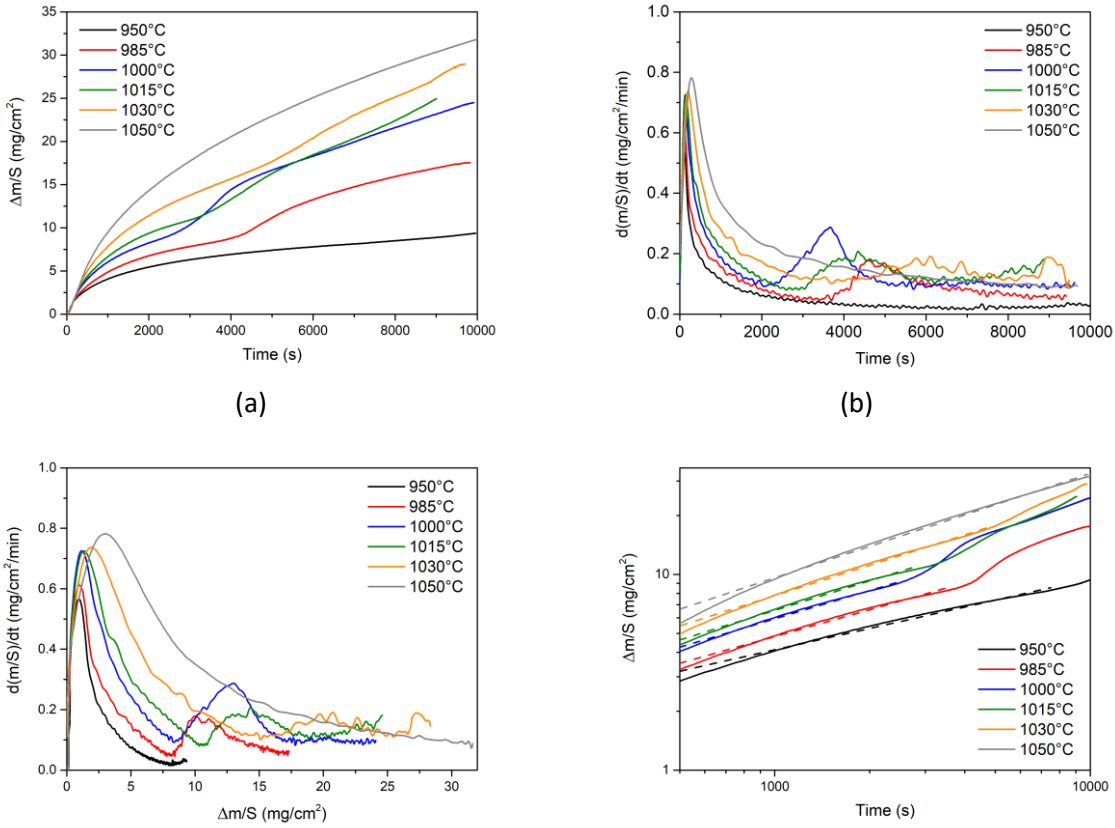

Figure 1 (a) Weight gain as function of time, (b) weight gain rate as a function of time, (c) weight gain rate as a function of weight gain and (d) weight gain as a function of time in a log-log scale at temperatures ranging from 950 to 1050 °C and 100 hPa of steam partial pressure.

Temperature (°C)	**950**	**985**	**1000***	**1015**	**1030**	**1050**
Exponent n	2.7	2.2	2.1	2	1.9	1.8
Transition time (s)	7300	3400	2700 ± 400	2900	3700	n/a
Weight gain at transition (mg/cm²)	8.2	8.1	9.1 ± 0.6	10.5	15.1	n/a

** The experiment at 1000 °C was repeated 20 times. The uncertainties represent the standard deviation of the results.*
Table 2 The exponent n, the transition times to breakaway oxidation and the corresponding weight gains at temperatures 950 to 1050 °C and 100 hPa of steam partial pressure.

Figure 2 shows an optical micrograph of a Zircaloy-4 sample oxidized at 1000 °C under 100 hPa of steam partial pressure during 10 000 s. Circumferential cracks caused by the breakaway oxidation cover the internal and external oxide formed. The brittle α-Zr(O) layer contains radial cracks formed either by creep of the underlying metal at high temperature or during the cooling phase.

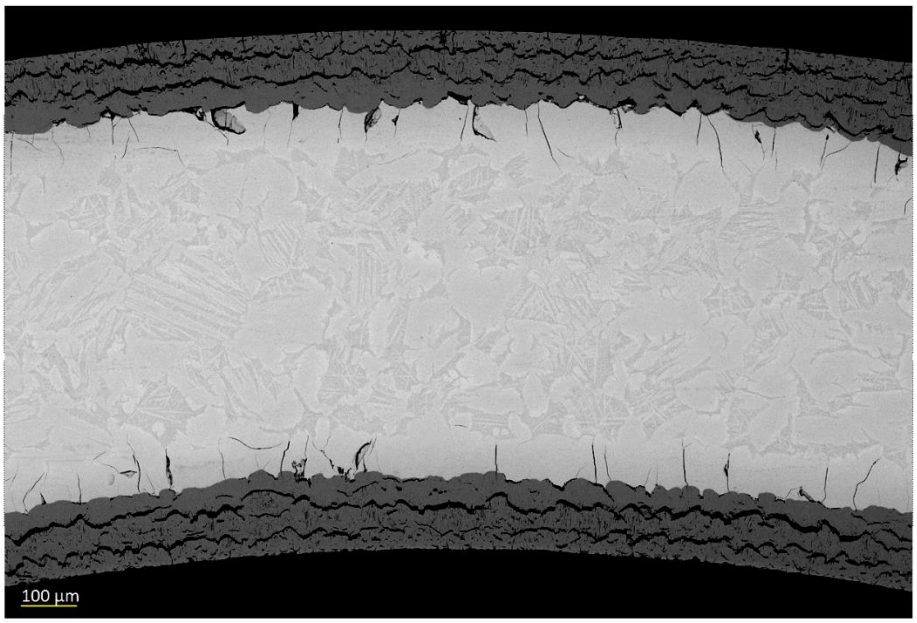

Figure 2 SEM micrograph of a polished sample oxidized at 1000 °C and 100 hPa of steam partial pressure during 10 000 s.

3.2. Rate determining step

Several tests were conducted with jumps in temperature from 1000 °C to 1030 °C with a heating rate of 30 °C/min at different extents of the reaction. Three examples of the resulting weight gain curves are presented in Figure 3. The dotted vertical lines mark the time at which 1030 °C was reached.

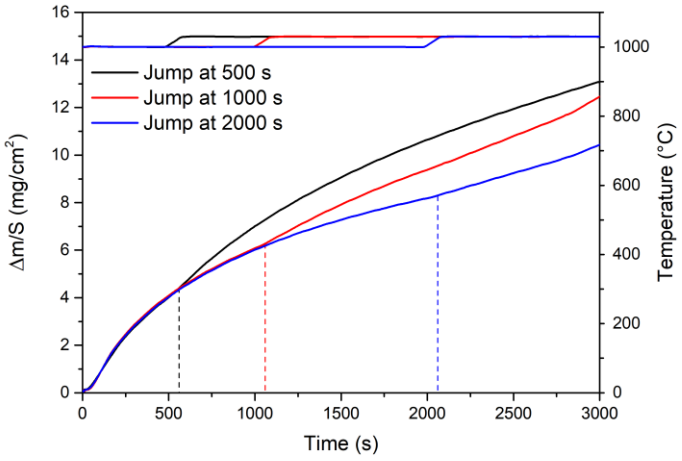

Figure 3 Weight gain curves showing three jumps in temperature from 1000 °C to 1030 °C at 500, 1000 and 2000 s in 100 hPa of steam partial pressure.

The results of the rate ratios resulting from all the temperature jumps are plotted in Figure 4. Three stages can be noticed: a pre-transition, a breakaway and a post-transition stage. In the pre- and post-transition stages, the rate ratios $\left(\frac{dm/S}{dt}\right)_{after\ jump} \Big/ \left(\frac{dm/S}{dt}\right)_{before\ jump}$ are approximately equal to a constant value of 1.25 ± 0.07. The error bars in Figure 4 represent the relative standard deviation of the values used to measure the rate ratios and are equal to $\pm \sqrt{\left(\frac{\sigma}{R}\right)^2_{before\ jump} + \left(\frac{\sigma}{R}\right)^2_{after\ jump}}$, therefore the increasing trend of the rate ratios obtained in the pre-transition regime should not be taken into account. The occurrence of breakaway oxidation induces important morphological changes

on the sample such as the formation of cracks in the oxide [5, 14, 36]. As a result, the changes in the function S_m during the temperature jumps can no longer be neglected, which leads to a deviation in the rate ratios at 3000 s and 3500 s as shown in Figure 4. We can conclude thus, that for the system studied in this paper, a rate-determining step exists in the pre- and post-transition stages for which the reaction rate can be expressed according to Eq. (1). However, the breakaway stage cannot be modeled using the same equation because of the induced microstructural changes in the oxide preventing the validation of Eq. (1) during this stage (leading to variable rate ratios as shown in Figure 4).

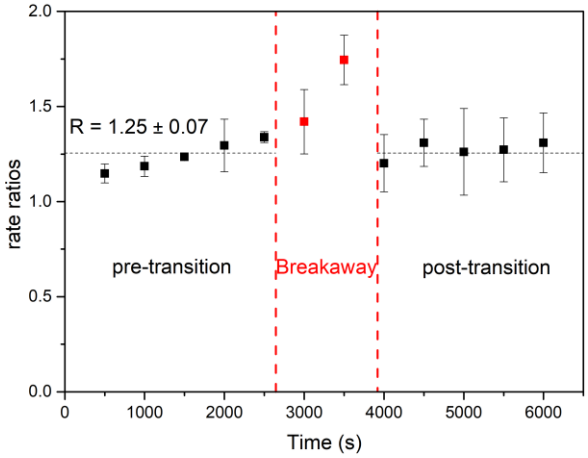

Figure 4 Rate ratios just before and just after the temperature jumps from 1000 °C to 1030 °C in 100 hPa of steam partial pressure.

3.3. Influence of thermodynamic parameters

3.3.1. Pre-transition

Figure 5 illustrates the kinetic curves obtained from the temperature jumps in the pre-transition stage. All the experiments started in the same experimental conditions, at 950 °C and 100 hPa of steam partial pressure. After 1000 s of isothermal oxidation, a temperature jump was programmed allowing the examination of six temperatures ranging from 985 to 1100 °C. All the curves are superimposed before carrying out the jumps (before 1000 s) showing thus the good reproducibility of the measures presented in this study. The reaction rate ratios measured just before and just after each jump from Figure 5 (b) correspond, according to Eq. (1), to the areic reactivity of growth ratios $\Phi(T_i, P_0)/\Phi(T_0, P_0)$ of the rate-determining step with P_0 and T_0 being the steam partial pressure and the temperature before the jump (100 hPa and 950 °C respectively) and T_i the temperature after the jump. The ratios $\Phi(T_i, P_0)/\Phi(T_0, P_0)$ increase exponentially with temperature following the Arrhenius law as shown in Figure 6 with an activation energy of 144 ± 5 kJ/mol. This value is close to the activation energy of the oxygen diffusivity in the oxide layer as reported by Debuigne [37] (140.5 kJ/mol), Iglesias *et al.* [38] (147 kJ/mol) and Ma *et al.* [39] (143.6 kJ/mol) (the activation energy of oxygen diffusivity in the α-Zr(O) layer being around 200 kJ/mol [8, 39]).

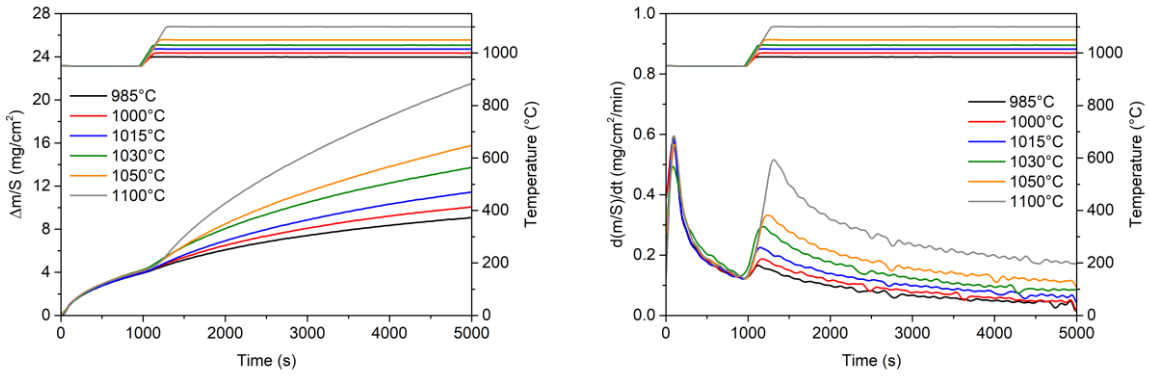

Figure 5 Temperature jumps during pre-transition stage from 950 °C to 985, 1000, 1015, 1030, 1050 and 1100 °C (in 100 hPa of steam partial pressure). (a) Weight gain curves and (b) weight gain rate curves.

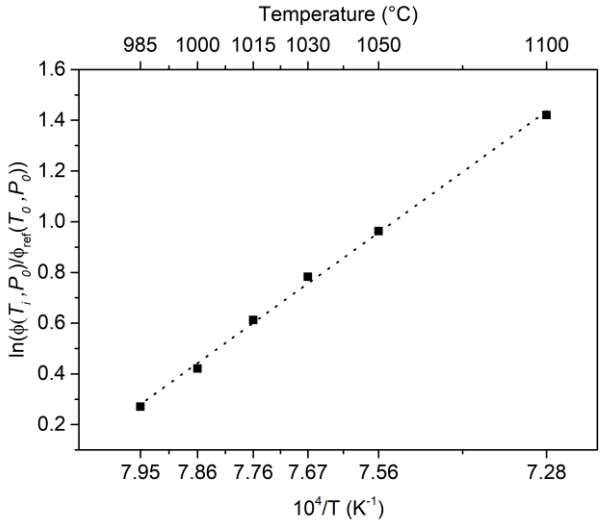

Figure 6 Arrhenius plot of $\Phi(T_i, P_0)/\Phi(T_0, P_0)$ at different temperatures in the pre-transition regime.

The influence of steam partial pressure was then examined by applying the same method. Four experiments were started in the same conditions at 1000 °C and 100 hPa of steam partial pressure. After 1000 s of isothermal oxidation, a jump in steam partial pressure was done increasing thus this parameter from 100 hPa to 110, 120, 130 and 140 hPa. The resulting weight gain curves illustrated in Figure 7 (a) are superimposed, which means that in the explored range of this study, steam partial pressure has little to no effect on the areic reactivity of growth of the reaction.

In order to evaluate the influence of hydrogen partial pressure on the overall reaction kinetics, three cases were investigated as shown in Figure 7 (b). The first case consisted of running the experiment without fixing the hydrogen partial pressure (marked by $p(H_2) = 0$ hPa). In the second case, hydrogen partial pressure was maintained at a constant value of 27 hPa all along the isothermal oxidation. Finally, in the third case a jump in hydrogen partial pressure from $p(H_2) = 0$ hPa to $p(H_2) = 27$ hPa was carried out after 2000 s of isothermal oxidation at 1000 °C. Superimposed kinetic curves indicated that the influence of hydrogen partial pressure on the areic reactivity of growth can be neglected.

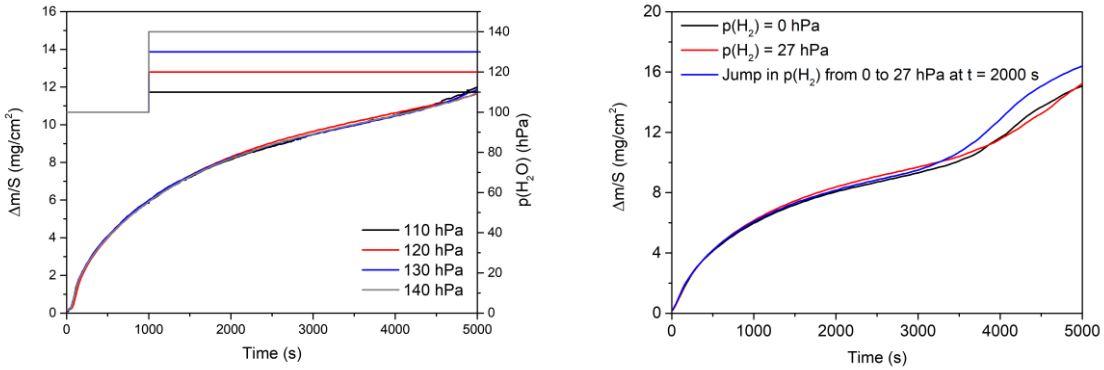

(a) (b)

Figure 7 (a) Weight gain curves resulting from the jumps in steam partial pressures at 1000 °C and (b) weight gain curves at different hydrogen partial pressures at 1000 °C in 100 hPa of steam partial pressure.

3.3.2. Post-transition

Since the results in Section 3.2 showed that a rate-determining step exists also in the post-transition regime, it was necessary to evaluate the influence of temperature, steam and hydrogen partial pressures on the areic reactivity of growth in this stage. Four experiments were conducted with the same starting conditions at 1000 °C and 100 hPa of steam partial pressure. Breakaway oxidation occurred around 2900 s as expected, highlighted by the increase of the reaction rate as illustrated in Figure 8. After 5500 s of isothermal oxidation, temperature jumps were carried out from 1000 °C to 950, 1015, 1030 and 1050 °C. It can be deduced from Figure 9 that the variation of the ratios $\Phi(T_i, P_0)/\Phi(T_0, P_0)$ with temperature follows the Arrhenius law with an activation energy of 146 ± 4 kJ/mol, equal to the value measured in the pre-transition stage.

The influence of steam and hydrogen partial pressures was also investigated applying pressure jumps at 5500 s. The resulting kinetic curves are superimposed indicating that the steam and hydrogen partial pressures have a negligible effect on the areic reactivity of growth of the reaction, similarly to that observed in the pre-transition stage.

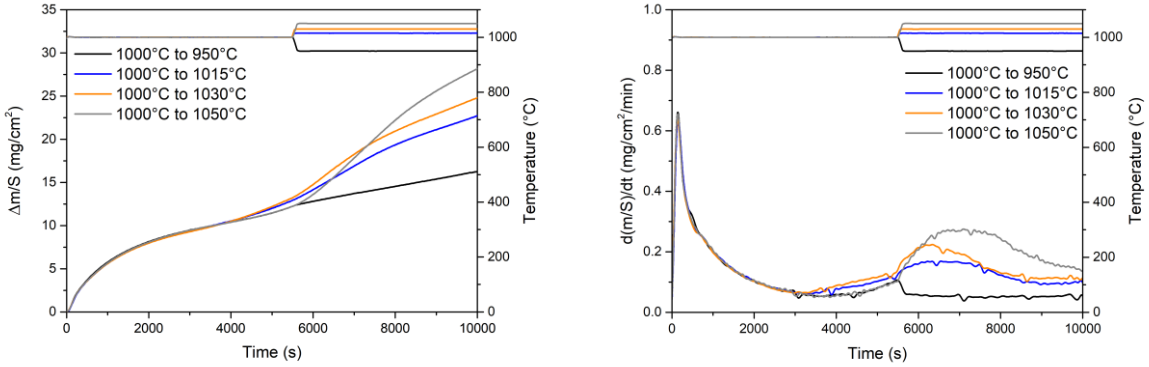

(a) (b)

Figure 8 Temperature jumps in the post-transition regime from 1000 °C to 950, 1015, 1030 and 1050 °C (in 100 hPa of steam partial pressure). Weight gain curves (a) and weight gain rate curves (b).

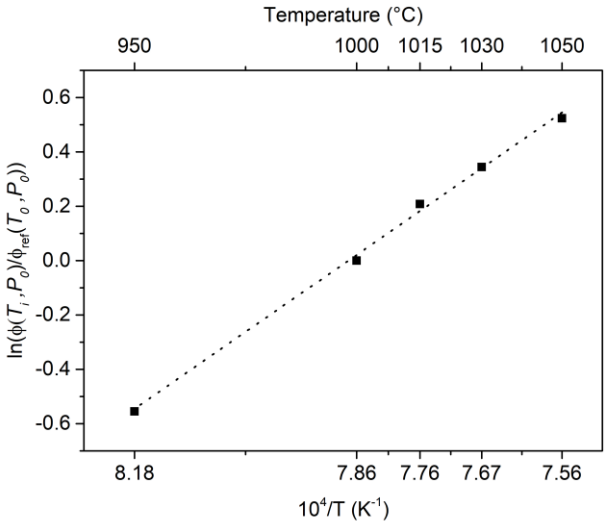

Figure 9 Arrhenius plot of $\Phi(T_i, P_0)/\Phi(T_0, P_0)$ at different temperatures in the post-transition regime.

4. Discussion

The results obtained in this study show that the overall reaction rate decreases with time according to the parabolic law, in both pre- and post-transition stages, indicating a possible rate-determining step of diffusion. We demonstrated then the existence of a rate-determining step using the method of jumps, and showed that steam and hydrogen partial pressures have a negligible effect on the areic reactivity of growth within the tested range of partial pressures. Taking into account these data, a mechanism with parallel steps [28] describing the inward growth of both the oxide and alpha layer in steam at high temperature, inspired by the mechanisms in [24, 40], can be proposed.

This mechanism is illustrated in Figure 10. It contains a common path including the steps (1)-(4) and 2 parallel branches. The first parallel branch corresponds to the oxide growth (5') and a second parallel branch describes the α-Zr(O) growth (5)-(7). In the next paragraph, the oxide/gas interface is referred to as external interface (ext), the oxide/α-Zr(O) interface as internal interface 1 $(int\ 1)$ and the α-Zr(O)/β_{Zr} as internal interface 2 $(int\ 2)$.

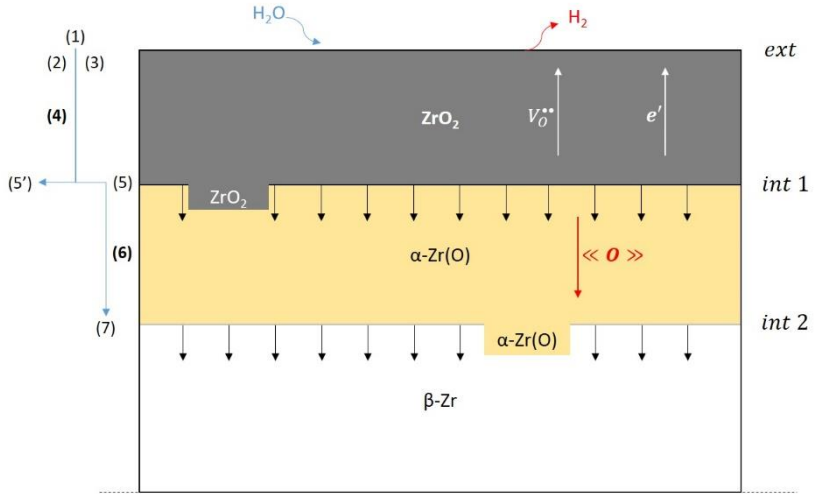

Figure 10 Schematic illustration of the mechanism describing the oxide and α-Zr(O) growth in steam at high-temperature

This translates into the following elementary steps using the Kröger-Vink notation [41]:

Step (1) Adsorption of steam on a surface site 's':

$$H_2O(g) + s \leftrightarrow H_2O - s$$

Step (2) Oxide/gas interface reaction:

$$H_2O - s \ + \mathrm{V}_{O}^{\bullet\bullet}{}_{ext} + 2\mathrm{e}' \leftrightarrow O_{O(ZrO_2)} + H_2 - s$$

Step (3) Hydrogen desorption:

$$H_2 - s \leftrightarrow H_2(g) + s$$

Step (4) Diffusion of oxygen vacancies and electrons:

$$V_{O}^{\bullet\bullet}{}_{int\,1} \rightarrow V_{O}^{\bullet\bullet}{}_{ext}$$

$$e'_{int\,1} \rightarrow e'_{ext}$$

Step (5) Oxide/α-Zr(O) interface reaction ($O_i^X{}_{int\,1}$ is an oxygen atom in an interstitial site in α-Zr(O)):

$$O_{O(ZrO_2)} + V_{i_{\alpha-Zr(O)}} \leftrightarrow O_i^X{}_{int\,1} + \mathrm{V}_{O}^{\bullet\bullet}{}_{int\,1} + 2e'$$

Step (5') Oxide/α-Zr(O) interface reaction

$$Zr_{Zr(\alpha-Zr(O))} \leftrightarrow Zr_{Zr(ZrO_2)}^X + 2\mathrm{V}_{O}^{\bullet\bullet}{}_{int\,1} + 4e'$$

Step (6) Diffusion of atomic oxygen in solid solution:

$$O_{i_{int\,1}} \leftrightarrow O_{i_{int\,2}}$$

Step (7) α-Zr(O)/β-Zr(O) interface reaction:

$$Zr_{Zr(\beta-Zr)} + O_{i_{int\,2}} \leftrightarrow Zr_{Zr(\alpha-Zr(O))} + \ll O \gg_{Metal}$$

The linear combination of the steps (1)-(5') [2] and (1)-(7)[3], each step multiplied by its corresponding λ_i (multiplying coefficient [28]), leads to the two global equations respectively:

Oxide growth:

$$Zr_{Zr(\alpha-Zr(O))} + 2H_2O(g) \leftrightarrow Zr_{Zr(ZrO_2)} + 2O_{O(ZrO_2)} + 2H_2(g) \quad (2)$$

α-Zr(O) growth:

$$Zr_{Zr(\beta-Zr)} + H_2O(g) \leftrightarrow Zr_{Zr(\alpha-Zr(O))} + \ll O \gg_{Metal} + H_2(g) \quad (3)$$

Two diffusion steps can be found in the proposed mechanism: the diffusion of oxygen vacancies in the oxide layer (step (4)) and the diffusion of atomic oxygen in solid solution in α-Zr(O) (step (6)). For simplicity reasons, the diffusion in this mechanism is considered to be governed by Fick's law. In order to solve the system of equations derived from the mechanism[4], the assumption of electroneutrality conservation was considered. The expressions of the areic reactivities of growth for the two diffusion steps can be deduced from the mechanism, each time considering that the other elementary steps are at equilibrium [31]:

$$\Phi_4 = \frac{D_{O/oxide}}{l_0}\frac{K_{5'}^{1/6}}{2^{2/3}}\left[1 - \left(\frac{p(H_2)}{K_{eq_{oxide}}^{1/2}p(H_2O)}\right)^{1/3}\right] \approx \frac{D_{O/oxide}}{l_0}\frac{K_{5'}^{1/6}}{2^{2/3}} \quad (4)$$

[2] For the linear combination of the steps (1)-(5'): $\lambda_{1-4} = 2$ and $\lambda_{5'} = 1$

[3] For the linear combination of the steps (1)-(7): $\lambda_{1-7} = 1$

[4] For further information and details explaining how to solve the system of equations please refer to references [28] (chapter 7) and [29].

$$\Phi_6 = \frac{D_{O/\alpha}}{l_0}\frac{K_1K_2K_3K_5p(H_2O)}{p(H_2)}\left[1-\frac{p(H_2)}{K_{eq_\alpha}p(H_2O)}\right] \approx \frac{D_{O/\alpha}}{l_0}\frac{K_1K_2K_3K_5p(H_2O)}{p(H_2)} \quad (5)$$

Where $D_{O/oxide}$ and $D_{O/\alpha}$ are the diffusion coefficients of oxygen in the oxide and in the α-Zr(O) layers respectively, K_i is the equilibrium constant of the i^{th} step, $K_{eq_{oxide}}$ and K_{eq_α} are the equilibrium constants of the Eq. (2) and Eq. (3) respectively and l_0 an arbitrary length = 1 m. The terms in brackets describe the gap between thermodynamic equilibrium conditions and experimental conditions, i.e. the direction in which the reactions in Eq. (2) and (3) proceed (from left to right). At 1000 °C the value of K_{eq} reported in several references [42] is around 3.8×10^{20} for pure zirconium meaning that the terms in brackets are approximately equal to 1.
The experimental results obtained in Section 2 allow us to identify which of the two steps (4) and (6) is the rate-determining step. In fact, it was demonstrated that the influences of steam and hydrogen partial pressures are negligible which means that step (4) or the diffusion of oxygen vacancies in the oxide layer is the rate-determining step. This also means that the activation energy obtained in section 3.3 is an apparent energy of activation that can be expressed as $E_{a_{apparent}} = E_{a_{D_{O/oxide}}} + \Delta H_{5'}$ according to Arrhenius and van't Hoff laws [28], with $\Delta H_{5'}$ being the enthalpy of the elementary step (5').

Since this rate-determining step belongs to the common branch, the other steps, including those in the parallel branches (5') and (5)-(7), should be at equilibrium and both Eq. (2) and Eq. (3) advance at proportional rates. Thus we can conclude from these two equations that for every three molecules of steam reacting with the metal, two serve the oxide growth and one serves the α-Zr(O) growth:

$$\frac{\Delta m_{oxide}}{S} \approx \frac{2}{3}\frac{\Delta m_{total}}{S} \quad (6)$$

$$\frac{\Delta m_{\alpha-Zr(O)}}{S} \approx \frac{1}{3}\frac{\Delta m_{total}}{S} \quad (7)$$

A way to verify the validity of the proposed mechanism in this study and the equations (6) and (7) is to evaluate how the experimental overall weight gain is distributed between the oxide and α-Zr(O) growth during isothermal oxidation. In order to do that, measurements of the oxide thickness were done at different times for a sample oxidized at 1000 °C in 100 hPa of steam partial pressure. Considering that the steady-state regime is maintained all along the isothermal oxidation, the oxide thickness can be transformed into a weight gain by using the following formula deduced from Eq. (2):

$$\frac{\Delta m_{oxide}}{S_0}(mg/cm^2) = 2.10^{-1}\rho_{ZrO_2}\frac{M_O}{M_{ZrO_2}}e_{oxide} \quad (8)$$

Where e_{oxide} is the oxide thickness (in µm), M_{ZrO_2} and M_O are the molar masses of zirconia and oxygen respectively (in g/mol), ρ_{ZrO_2} is the density of zirconia (in g/cm^3), Δm_{oxide} is the theoretical weight gain needed to obtain a zirconia thickness (in mg) of e_{oxide} and S_0 the external surface of the sample (in cm^2).

Oxide and α-Zr(O) thicknesses were measured by optical microscopy at the end of seven experiments carried out at the same conditions, at 1000 °C and 100 hPa of steam partial pressure during 120, 2000, 2700, 4000, 5000, 10 000 and 15 000 s.

Figure 11 illustrates the thickness variation of the external oxide and α-Zr(O) layers with time. The thicknesses seem to increase similarly at the beginning of the isothermal oxidation. A faster increase in the oxide thickness is then observed from 2700 s caused by the breakaway oxidation.

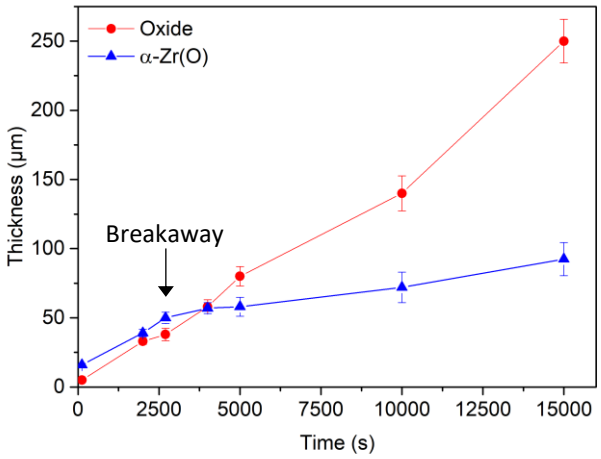

Figure 11 Measured thicknesses of the oxide and α-Zr(O) layers with time at 1000 °C and 100 hPa of steam partial pressure.

The comparison of the weight gain deduced from the thickness of the oxide layer (Eq. (8)) and the weight gain deduced from the proposed mechanism (Eq. (6)) is illustrated in Figure 12. We can clearly see that the two sets of results fit well together for times less than 10000 s, confirming the validity of the mechanism and the resulting Eq. (2) and (3).

For times longer than 10000 s, the oxide weight gain measured by Eq. (6) is lower than the experimental value, indicating a possible change in the mechanism. In order to verify this assumption, it was necessary to evaluate the variation of the weight gain contributing to the growth of the α-Zr(O) layer with time. In case of the oxide, Eq. (8) was used because the oxygen gradient in the oxide scale can be considered as negligible. However, the oxide gradient in the α-Zr(O) layer is important, ranging from 10 %at. to 29 %at. [43], and cannot be neglected. Nevertheless, since we have the total weight gain obtained by thermogravimetry and the weight gain corresponding to the growth of the oxide (Eq. (8)), we can deduce by simple subtraction, the contribution of the weight gain serving the growth of the α-Zr(O) layer.

$$\frac{\Delta m_{\alpha-Zr(O)}}{S} = \frac{\Delta m_{total}}{S} - \frac{\Delta m_{oxide}}{S} \tag{9}$$

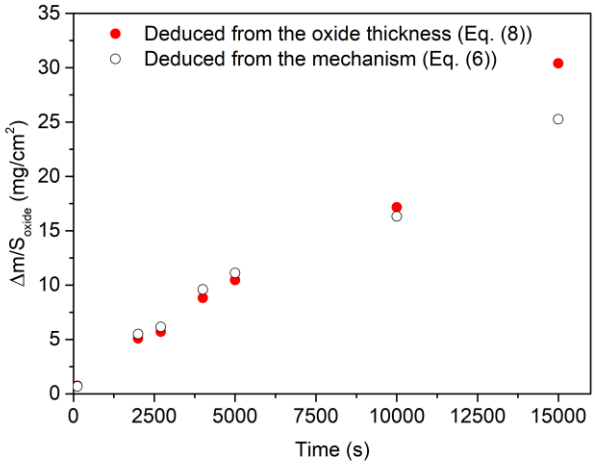

Figure 12 Comparison of experimental and theoretical weight gain corresponding only to the oxide growth.

It is important to note that the weight gain corresponding to the growth of the α-Zr(O) obtained by Eq. (9) could give a higher weight gain than that measured from the continuous α-Zr(O) thickness with an average oxygen concentration. The continuous α-Zr(O) layer does not take into account the oxygen

present in the intermediate α-Zr(O) + β-Zr layer, which means that measuring the α-Zr(O) weight gain from its continuous thickness could be misleading.
The corresponding weight gain variation of the oxide and α-Zr(O) layers are presented in Figure 13. It can be clearly seen that from the beginning of the isothermal oxidation until 5000 s, the evolution of the three curves is relatively similar. A deviation in the α-Zr(O) weight gain curve can be noticed for times higher than 5000 s, marked by a much slower increase. This means that after 5000 s, almost the totality of the oxygen absorbed by the sample goes to the oxidation of the zirconium described by Eq. (2), and the quantity of oxygen in the α-Zr(O) layer becomes almost constant (even before the total consumption of the β-Zr phase). As a result, a change in the mechanism occurs, shifting from a mechanism with parallel steps to a linear one containing only steps (1)-(5').
The continuous increase in the α-Zr(O) thickness observed in Figure 11 after 5000 s, even though the corresponding weight gain becomes almost constant, could be the result of oxygen saturation in the β-Zr phase changing thus the oxygen gradient between the oxide/α-Zr(O) interface and the α-Zr(O)/β-Zr interface. In other terms, the diffusion mode shifts from a diffusion in a semi-infinite medium to a diffusion in a finite medium. Further investigations are necessary to fully confirm this hypothesis.

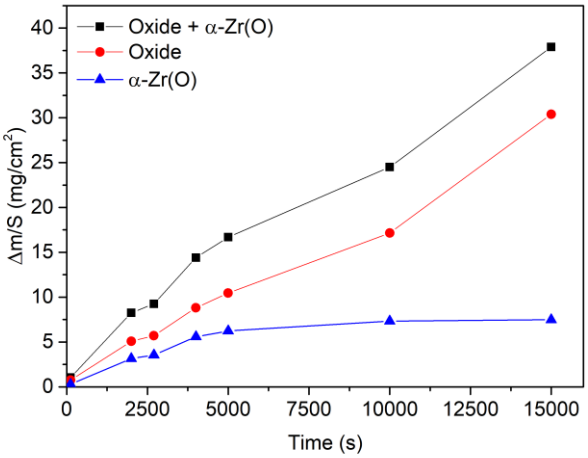

Figure 13 Weight gain distribution with time at 1000 °C and 100 hPa of steam partial pressure.

5. Conclusion

The kinetic behavior of Zircaloy-4 in a mixture of steam and helium at temperatures ranging from 950 to 1050 °C was studied. The occurrence of the breakaway oxidation in the studied temperature range was in accordance with the literature. A similar behavior was observed in the pre- and post-transition regimes where a rate-determining step controls the overall reaction kinetics. The variation of the areic reactivity of growth with temperature, steam and hydrogen partial pressures indicate a possible rate-determining step of diffusion of the oxygen vacancies in the oxide layer.

A detailed mechanism with parallel steps was proposed describing the growth of both oxide and α-Zr(O) layers. This mechanism allowed getting access to the weight gain distribution, quantifying thus the weight gain corresponding to the growth of each of the oxide and α-Zr(O) layers.

It was demonstrated that for times longer than 10000 s, the mechanism shifts from parallel to linear meaning that the reaction describing the growth of the α-Zr(O) layer reaches equilibrium state. Consequently, the majority of the newly reacted steam leads only to the growth of the zirconia layer. This last assumption can be verified by studying, in the same conditions, the variation of the oxygen gradient within the α-Zr(O) layer at different oxidation times.

Longer oxidation times will be investigated, reaching total consumption of the metal, in order to verify any possible change in the rate-determining step. The evaluation of the function $S_m(t)$ will also be investigated to offer a complete kinetic model describing the oxidation reaction of Zircaloy-4 in steam at high temperatures.

Acknowledgements

This PhD is supported by a CIFRE project N°2017/1016 and we thank the ANRT for their logistic and financial support.

References

[1] U. N. R. Commission and others, 'Standard Review Plan, 4.2 Fuel System Design', *NUREG-0800*, 2007.

[2] K. Pettersson *et al.*, 'Nuclear Fuel Behaviour in Loss-of-coolant Accident (LOCA) Conditions', Organisation for Economic Co-Operation and Development, 2009.

[3] L. Baker and L. C. Just, 'Studies of metal-water reactions at high temperatures III. Experimental and theoretical studies of the zirconium-water reaction', *ANL-6548 Argonne Natl. Lab.*, vol. 406, 1962.

[4] S. Leistikow and G. Schanz, 'Oxidation kinetics and related phenomena of zircaloy-4 fuel cladding exposed to high temperature steam and hydrogen-steam mixtures under PWR accident conditions', *Nucl. Eng. Des.*, vol. 103, no. 1, pp. 65–84, 1987, doi: https://doi.org/10.1016/0029-5493(87)90286-X.

[5] S. Leistikow and S. Schanz, 'The oxidation behavior of Zircaloy-4 in steam between 600 and 1600° C', *Mater. Corros.*, vol. 36, no. 3, pp. 105–116, 1985.

[6] V. F. Urbanic and T. R. Heidrick, 'High-temperature oxidation of zircaloy-2 and zircaloy-4 in steam', *J. Nucl. Mater.*, vol. 75, no. 2, pp. 251–261, Aug. 1978, doi: 10.1016/0022-3115(78)90006-5.

[7] T. Furuta and S. Kawasaki, 'Reaction behavior of zircaloy-4 in steam-hydrogen mixtures at high temperature', *J. Nucl. Mater.*, vol. 105, no. 2, pp. 119–131, 1982, doi: https://doi.org/10.1016/0022-3115(82)90366-X.

[8] R. Pawel, J. Cathcart, and R. McKee, 'The Kinetics of Oxidation of Zircaloy-4 in Steam at High Temperatures', *J. Electrochem. Soc.*, vol. 126, no. 7, pp. 1105–1111, 1979.

[9] G. Schanz, S. Leistikow, and H. Uetsuka, 'Investigations of zircaloy-4 cladding oxidation under steam starvation and hydrogen blanketing conditions', 1984.

[10] F. Nagase, T. Otomo, and H. Uetsuka, 'Oxidation kinetics of low-Sn Zircaloy-4 at the temperature range from 773 to 1,573 K', *J. Nucl. Sci. Technol.*, vol. 40, no. 4, pp. 213–219, 2003.

[11] M. Steinbrück and M. Böttcher, 'Air oxidation of Zircaloy-4, M5® and ZIRLO™ cladding alloys at high temperatures', *J. Nucl. Mater.*, vol. 414, no. 2, pp. 276–285, 2011.

[12] B. Cox, 'Some thoughts on the mechanisms of in-reactor corrosion of zirconium alloys', *J. Nucl. Mater.*, vol. 336, no. 2–3, pp. 331–368, 2005.

[13] S. Leistikow, G. Schanz, H. Berg, and A. Aly, 'Comprehensive presentation of extended Zircaloy-4 steam oxidation results (600-1600 deg. C)', 1983.

[14] M. Billone, Y. Yan, T. Burtseva, R. Daum, and others, 'Cladding embrittlement during postulated loss-of-coolant accidents.', Argonne National Laboratory (ANL), 2008.

[15] J. H. Baek and Y. H. Jeong, 'Breakaway phenomenon of Zr-based alloys during a high-temperature oxidation', *J. Nucl. Mater.*, vol. 372, no. 2, pp. 152–159, 2008, doi: https://doi.org/10.1016/j.jnucmat.2007.02.011.

[16] K. Park, K. Kim, T. Yoo, and K. Kim, 'Pressure effects on high temperature steam oxidation of zircaloy-4', *Met. Mater. Int.*, vol. 7, no. 4, pp. 367–373, Jul. 2001, doi: 10.1007/BF03186081.

[17] J. H. Baek, K. B. Park, and Y. H. Jeong, 'Oxidation kinetics of Zircaloy-4 and Zr–1Nb–1Sn–0.1Fe at temperatures of 700–1200°C', *J. Nucl. Mater.*, vol. 335, no. 3, pp. 443–456, 2004, doi: https://doi.org/10.1016/j.jnucmat.2004.08.007.

[18] R. Zino, R. Chosson, M. Ollivier, and E. Serris, 'Breakaway characterization of Zircaloy-4 oxidized in steam and in oxygen at high temperatures using HT- XRD analysis', *Corros. Sci.*, vol. 176, p. 109028, 2020, doi: https://doi.org/10.1016/j.corsci.2020.109028.

[19] J. Böhmert, M. Dietrich, and J. Linek, 'Comparative studies on high-temperature corrosion of ZrNb1 and Zircaloy-4', *Nucl. Eng. Des.*, vol. 147, no. 1, pp. 53–62, 1994.

[20] H. E. Kadiri *et al.*, 'Transformations and cracks in zirconia films leading to breakaway oxidation of Zircaloy', *Acta Mater.*, vol. 61, no. 11, pp. 3923–3935, 2013, doi: https://doi.org/10.1016/j.actamat.2013.02.052.

[21] D. J. Park, J. Y. Park, Y. H. Jeong, and J. Y. Lee, 'Microstructural characterization of ZrO2 layers formed during the transition to breakaway oxidation', *J. Nucl. Mater.*, vol. 399, no. 2, pp. 208–211, 2010, doi: https://doi.org/10.1016/j.jnucmat.2010.01.021.

[22] L. Keys, G. Beranger, B. De Gélas, and P. Lacombe, 'Etude micrographique du processus de desquamation ("break-away") au cours de l'oxydation du zirconium', *J. Common Met.*, vol. 14, no. 2, pp. 181–200, 1968.
[23] R. E. Pawel, J. V. Cathcart, and J. J. Campbell, 'The oxidation of zircaloy-4 at 900 and 1100°c in high pressure steam', *J. Nucl. Mater.*, vol. 82, no. 1, pp. 129–139, 1979, doi: https://doi.org/10.1016/0022-3115(79)90045-X.
[24] M. Tupin, M. Pijolat, F. Valdivieso, M. Soustelle, A. Frichet, and P. Barberis, 'Differences in reactivity of oxide growth during the oxidation of Zircaloy-4 in water vapour before and after the kinetic transition', *J. Nucl. Mater.*, vol. 317, no. 2–3, pp. 130–144, 2003.
[25] Y. Dali, M. Tupin, P. Bossis, M. Pijolat, Y. Wouters, and F. Jomard, 'Corrosion kinetics under high pressure of steam of pure zirconium and zirconium alloys followed by in situ thermogravimetry', *J. Nucl. Mater.*, vol. 426, no. 1–3, pp. 148–159, 2012.
[26] M. Lasserre-Gagnaire, 'Modélisation des phénomènes de corrosion du Zircaloy-4 sous mélanges oxygène-azote à haute température', PhD Thesis, 2013.
[27] M. Gestin *et al.*, 'Experimental study of oxidation in oxygen, nitrogen and steam mixtures at 850∘C of pre-oxidized Zircaloy-4', *J. Nucl. Mater.*, vol. 519, pp. 302–314, 2019, doi: https://doi.org/10.1016/j.jnucmat.2019.03.020.
[28] M. Soustelle, *Heterogeneous kinematics handbook*. ISTE/Wiley, 2010.
[29] M. Pijolat and L. Favergeon, 'Chapter 5 - Kinetics and Mechanisms of Solid-Gas Reactions', in *Recent Advances, Techniques and Applications*, vol. 6, S. Vyazovkin, N. Koga, and C. Schick, Eds. Elsevier Science B.V., 2018, pp. 173–212.
[30] M. Pijolat and M. Soustelle, 'Experimental tests to validate the rate-limiting step assumption used in the kinetic analysis of solid-state reactions', *Thermochim. Acta*, vol. 478, no. 1–2, pp. 34–40, 2008.
[31] M. Soustelle and M. Pijolat, 'Experimental methods useful in the kinetic modelling of heterogeneous reactions', *Solid State Ion.*, vol. 95, no. 1–2, pp. 33–40, 1997.
[32] J. Cathcart *et al.*, 'Zirconium metal-water oxidation kinetics. IV. Reaction rate studies', Oak Ridge National Lab., 1977.
[33] L. Portier, T. Bredel, J. Brachet, V. Maillot, J. Mardon, and A. Lesbros, 'Influence of Long Service Exposures on the Thermal-Mechanical Behavior of Zy-4 and M5^{TM} Alloys in LOCA Conditions', in *Zirconium in the Nuclear Industry: Fourteenth International Symposium*, 2005.
[34] M. Grosse, 'Comparison of the High-Temperature Steam Oxidation Kinetics of Advanced Cladding Materials', *Nucl. Technol.*, vol. 170, no. 1, pp. 272–279, Apr. 2010, doi: 10.13182/NT10-A9464.
[35] M. Steinbrück, N. Vér, and M. Grosse, 'Oxidation of Advanced Zirconium Cladding Alloys in Steam at Temperatures in the Range of 600–1200 °C', *Oxid. Met.*, vol. 76, no. 3, pp. 215–232, Oct. 2011, doi: 10.1007/s11085-011-9249-3.
[36] H.-G. Kim, I.-H. Kim, B.-K. Choi, and J.-Y. Park, 'A study of the breakaway oxidation behavior of zirconium cladding materials', *J. Nucl. Mater.*, vol. 418, no. 1, pp. 186–197, 2011, doi: https://doi.org/10.1016/j.jnucmat.2011.06.039.
[37] J. Debuigne, *Contribution à l'étude de l'oxydation du zirconium et de la diffusion de l'oxygène dans l'oxyde et dans le métal...* Éditions Métaux, 1966.
[38] F. C. Iglesias, D. B. Duncan, S. Sagat, and H. E. Sills, 'Verification of the from model for zircaloy oxidation during high temperature transients', *J. Nucl. Mater.*, vol. 130, pp. 36–44, 1985, doi: https://doi.org/10.1016/0022-3115(85)90292-2.
[39] X. Ma, C. Toffolon-Masclet, T. Guilbert, D. Hamon, and J. C. Brachet, 'Oxidation kinetics and oxygen diffusion in low-tin Zircaloy-4 up to 1523K', *J. Nucl. Mater.*, vol. 377, no. 2, pp. 359–369, Jul. 2008, doi: 10.1016/j.jnucmat.2008.03.012.
[40] Y. Wouters, A. Galerie, and J.-P. Petit, 'Thermal oxidation of titanium by water vapour', *Solid State Ion.*, vol. 104, no. 1–2, pp. 89–96, 1997.
[41] F. A. Kröger, 'The chemistry of imperfect crystals', North-Holland Pub. Co.;, 1964.
[42] C. W. Bale *et al.*, 'FactSage thermochemical software and databases, 2010–2016', *Calphad*, vol. 54, pp. 35–53, 2016, doi: https://doi.org/10.1016/j.calphad.2016.05.002.

[43] N. Dupin, I. Ansara, C. Servant, C. Toffolon, C. Lemaignan, and J. Brachet, ‘A thermodynamic database for zirconium alloys’, *J. Nucl. Mater.*, vol. 275, no. 3, pp. 287–295, 1999.